

Structural and Biochemical Evidence for an Autoinhibitory Role for Tyrosine 984 in the Juxtamembrane Region of the Insulin Receptor*

Received for publication, March 10, 2003, and in revised form, April 14, 2003
Published, JBC Papers in Press, April 21, 2003, DOI 10.1074/jbc.M302425200

Shiqing Li, Nicole D. Covino, Evan G. Stein, Jeffrey H. Till‡, and Stevan R. Hubbard§

From the Skirball Institute of Biomolecular Medicine and Department of Pharmacology, New York University School of Medicine, New York, New York 10016

Tyrosine 984 in the juxtamembrane region of the insulin receptor, between the transmembrane helix and the cytoplasmic tyrosine kinase domain, is conserved among all insulin receptor-like proteins from hydra to humans. Crystallographic studies of the tyrosine kinase domain and proximal juxtamembrane region reveal that Tyr-984 interacts with several other conserved residues in the N-terminal lobe of the kinase domain, stabilizing a catalytically nonproductive position of α -helix C. Steady-state kinetics measurements on the soluble kinase domain demonstrate that replacement of Tyr-984 with phenylalanine results in a 4-fold increase in k_{cat} in the unphosphorylated (basal state) enzyme. Moreover, mutation of Tyr-984 in the full-length insulin receptor results in significantly elevated receptor phosphorylation levels in cells, both in the absence of insulin and following insulin stimulation. These data demonstrate that Tyr-984 plays an important structural role in maintaining the quiescent, basal state of the insulin receptor. In addition, the structural studies suggest a possible target site for small molecule activators of the insulin receptor, with potential use in the treatment of noninsulin-dependent diabetes mellitus.

The insulin receptor is a member of the receptor tyrosine kinase (RTK)¹ family of cell surface receptors. Unlike the majority of RTKs, which are monomeric in the absence of ligand, the insulin receptor is a disulfide-linked heterotetramer comprising two extracellular α subunits and two membrane-spanning β subunits (1, 2). Upon insulin binding to the α subunits, the insulin receptor undergoes a poorly characterized structural rearrangement that facilitates autophosphorylation of specific tyrosine residues in the cytoplasmic portion of the β subunits. Tyrosine autophosphorylation stimulates receptor

catalytic (tyrosine kinase) activity (3) and creates recruitment sites for downstream signaling molecules such as the insulin receptor substrate (IRS) proteins (4) and APS (5).

Three tyrosine residues in the cytoplasmic juxtamembrane region of the insulin receptor, Tyr-965, Tyr-972, and Tyr-984, are conserved to various extents in the insulin receptor subfamily of RTKs (Fig. 1). This subfamily includes the insulin receptor, the insulin-like growth factor-1 (IGF1) receptor, the insulin receptor-related receptor (IRR), and insulin receptor-like proteins in invertebrates such as Daf-2 in *Caenorhabditis elegans* and DIR in *Drosophila melanogaster*. Tyr-965, an autophosphorylation site that is not conserved in the invertebrate receptors, appears to be involved in receptor endocytosis (6, 7). Tyr-972, invariant in the insulin receptor subfamily, is an essential autophosphorylation site (NPXY motif) that recruits IRS proteins (4), Shc (8), and Stat-5b (9) via a phosphotyrosine-binding domain in these adapter proteins. Tyr-984 is also invariant in this subfamily, yet its role in insulin receptor signaling has not been determined. Biochemical studies indicate that Tyr-984 is not, to any appreciable extent, a site of autophosphorylation (10, 11).

Previous crystallographic studies on the tyrosine kinase domain of the insulin receptor (IRK) have elucidated the mechanism by which *trans*-autophosphorylation of tyrosines in the kinase activation loop stimulates catalytic activity (12, 13). These studies were performed using a cytoplasmic domain construct comprising the core tyrosine kinase domain (residues 989–1283) and the juxtamembrane region proximal to the kinase domain (residues 978–988). This original construct included two amino acid substitutions in the kinase-proximal juxtamembrane region, Cys-981 \rightarrow Ser and Tyr-984 \rightarrow Phe. Cys-981, which is not conserved even among mammalian insulin receptors, was substituted with serine to prevent formation of disulfide-linked dimers *in vitro*. At the time of the initial structural studies, it was unclear whether Tyr-984 was an autophosphorylation site, and to avoid potential autophosphorylation heterogeneity, this tyrosine was substituted with phenylalanine. Use of the Tyr-984 \rightarrow Phe IRK protein (IRK^{Y984F}) in past structural studies, and the disordered state of Phe-984 therein, has left obscure the function of this conserved tyrosine.

To elucidate the role of Tyr-984 in insulin receptor function, we have determined a crystal structure of unphosphorylated IRK containing wild-type Tyr-984. Although crystals of wild-type IRK were obtained, the N-terminal kinase lobe in this crystal form is poorly ordered, and the position of Tyr-984 could not be ascertained. Crystals of a mutant IRK in which conserved Asp-1132 in the catalytic loop was substituted with asparagine (IRK^{D1132N}) diffract to high resolution, and a structure of this protein has been determined at 1.9 Å resolution. In this crystal structure, Tyr-984 is involved in several hydrophobic and hydrogen-bonding interactions with residues in α -helix C (α C) and in the five-stranded β sheet in the N-terminal lobe

* This work was supported by National Institutes of Health Grant DK52916 (to S. R. H.). Financial support for Beamline X12C of the National Synchrotron Light Source comes principally from the National Institutes of Health and the Department of Energy. The costs of publication of this article were defrayed in part by the payment of page charges. This article must therefore be hereby marked "advertisement" in accordance with 18 U.S.C. Section 1734 solely to indicate this fact.

The atomic coordinates and structure factors (code 1P14) have been deposited in the Protein Data Bank, Research Collaboratory for Structural Bioinformatics, Rutgers University, New Brunswick, NJ (<http://www.rcsb.org/>).

‡ Present address: Exelixis, Inc., South San Francisco, CA 94083.

§ To whom correspondence should be addressed: Skirball Institute of Biomolecular Medicine, New York University School of Medicine, 540 First Ave., New York, NY 10016. Tel.: 212-263-8938; Fax: 212-263-8951; E-mail: hubbard@saturn.med.nyu.edu.

¹ The abbreviations used are: RTK, receptor tyrosine kinase; IRS, insulin receptor substrate; IGF1, insulin-like growth factor-1; IRR, insulin receptor-related receptor; IRK, tyrosine kinase domain of the insulin receptor; HEK, human embryonic kidney.

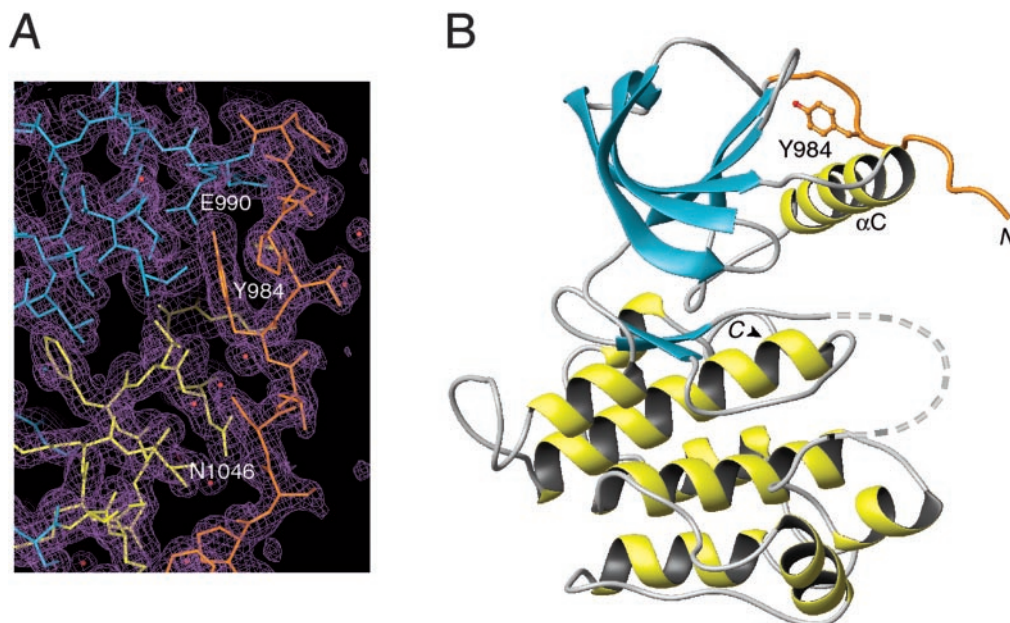


FIG. 2. **Crystal structure of IRK^{D1132N}.** *A*, $2F_o - F_c$ electron density map (1.9 Å resolution, 1σ contour) is shown in wire mesh (purple) in the region of Tyr-984. The superimposed refined structure of IRK^{D1132N} is shown in stick representation, with the proximal juxtamembrane region (residues 978–988) colored orange, residues in αC colored yellow, and residues in the β sheet (and connecting loops) colored cyan. Ordered water molecules are indicated with red spheres. Selected residues are labeled. *B*, ribbon diagram of the IRK^{D1132N} structure. β strands are colored cyan, and α -helices are colored yellow. The proximal juxtamembrane region including Tyr-984 is colored orange, with the side chain of Tyr-984 shown in ball-and-stick representation, and αC in the N-terminal lobe is labeled. The dashed gray line indicates that the activation loop is disordered (from Met-1153 through Leu-1171). The N and C termini are denoted by N and C.

resolution. A $2F_o - F_c$ electron density map in the vicinity of Tyr-984 is shown in Fig. 2A, and a ribbon diagram of the structure appears in Fig. 2B. The data collection and refinement statistics are given in Table I.

In the original crystal structure of unphosphorylated IRK (12), the activation loop traverses the cleft between the N- and C-terminal lobes of the kinase, and Tyr-1162 in the activation loop functions as a pseudosubstrate inhibitor, hydrogen-bonded to conserved Asp-1132 and Arg-1136 in the catalytic loop. This activation loop conformation, which occludes the active site, is representative of a “gate-closed” conformation (22). In the IRK^{D1132N} structure, the substitution of asparagine for Asp-1132 in the catalytic loop disrupts hydrogen bonding between Asp-1132 and Tyr-1162, leading to a “gate-open” conformation in which the activation loop is disengaged from the active site and mostly disordered (Fig. 2B). IRK^{D1132N} has negligible catalytic activity, however, because of the critical role of Asp-1132 in the phosphoryl transfer mechanism (23). The overall structure of IRK^{D1132N} is similar to the structure of another IRK mutant, Asp-1161 \rightarrow Ala, in which loss of four hydrogen bonds mediated by Asp-1161 in the activation loop is responsible for switching the activation loop conformation from gate-closed to gate-open (15). The gate-open conformation observed in the IRK^{D1132N} crystal structure is in agreement with solution studies that monitored the accessibility of the active site in this and other IRK mutants (23).

The conformation of the juxtamembrane region proximal to the kinase domain (residues 978–988) in the IRK^{D1132N} structure differs appreciably from those in IRK structures reported previously. In the IRK^{D1132N} structure, this segment lies along αC in the N-terminal kinase lobe (Figs. 2B and 3A). Tyr-984 is partially buried in a hydrophobic pocket formed at the junction between the five-stranded anti-parallel β sheet and αC in the N-terminal lobe (Fig. 3A). In addition to hydrophobic contacts between Tyr-984 and Leu-1045 and Val-1065, the hydroxyl group of Tyr-984 is hydrogen-bonded to Glu-990, another invariant residue in the insulin receptor subfamily. Glu-990 is also hydrogen-bonded to invariant Ser-1067.

TABLE I
X-ray data collection and refinement statistics

Data collection	
Resolution (Å)	30.0–1.9
Observations	149,169
Unique reflections	29,657
Completeness (%)	100.0 (100.0) ^a
R_{sym} (%) ^b	4.2 (29.8) ^a
Refinement ^c	
Resolution (Å)	25.0–1.9
Reflections	27,883
$R_{\text{cryst}}/R_{\text{free}}$ (%) ^d	22.5/24.1
Root mean square deviations	
Bond lengths (Å)	0.005
Bond angles (°)	1.3
B-factors (Å ²) ^e	0.87
Average B-factors (Å ²)	
All atoms	27.7
Protein	27.2
Water	33.6

^a The value in parentheses is for the highest resolution shell (1.94–1.90 Å).

^b $R_{\text{sym}} = 100 \times \sum |I - \langle I \rangle| / \sum I$.

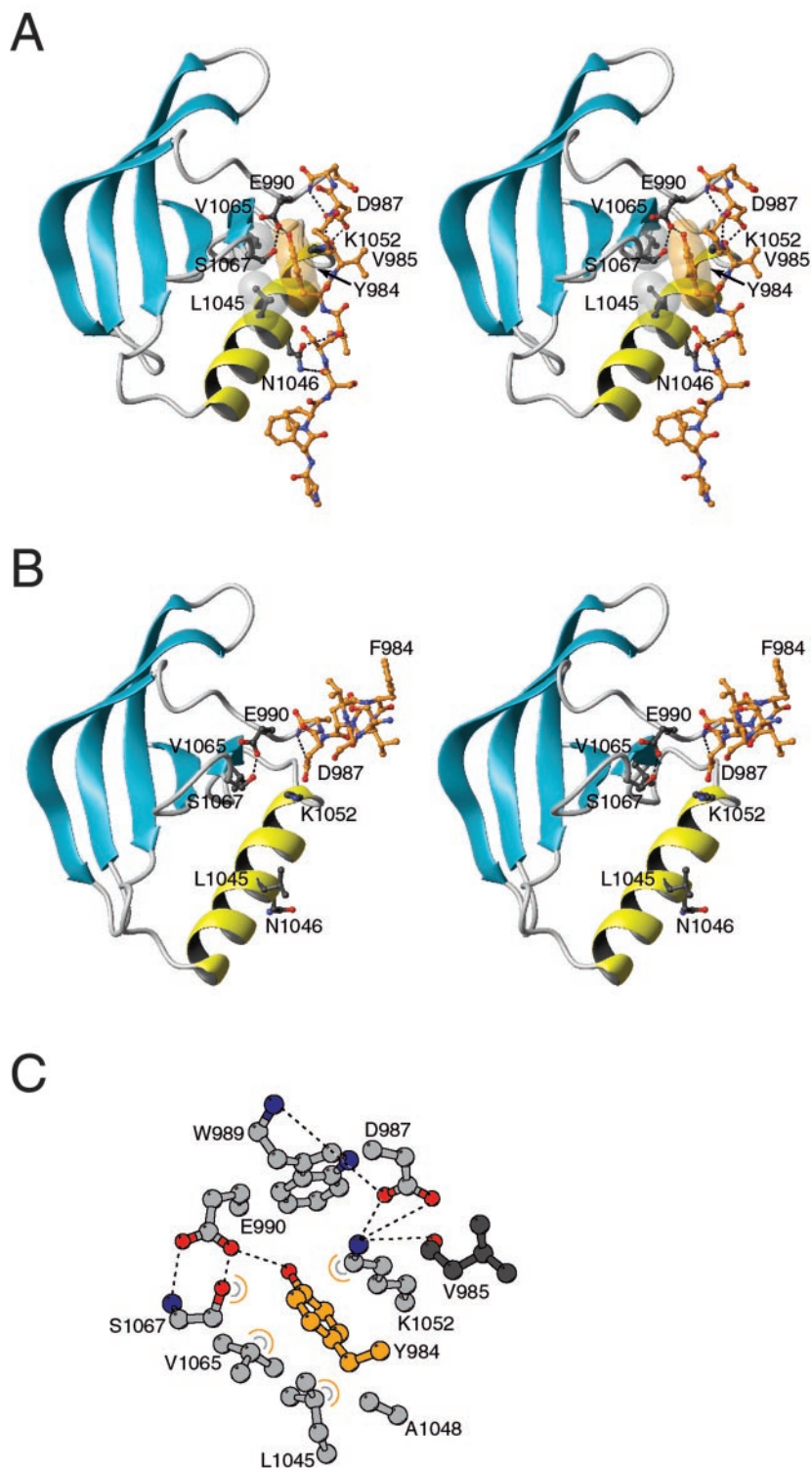
^c Atomic model includes 2233 protein atoms and 188 water molecules.

^d $R_{\text{cryst}} = 100 \times \sum \|F_o\| - \|F_c\| / \sum \|F_o\|$, where F_o and F_c are the observed and calculated structure factors, respectively ($F_o > 0\sigma$). R_{free} was determined from 5% of the data.

^e For bonded protein atoms.

In fact, a cluster of conserved residues in the insulin receptor subfamily is located in the junction between the juxtamembrane region and the kinase domain: Tyr-984, Asp-987, Trp-989, Glu-990, Ala-1048, Lys-1052, and Ser-1067 (Fig. 3C). In the IRK^{D1132N} structure, Lys-1052 (αC) participates in three hydrogen bonds with juxtamembrane residues, two with the side chain of Asp-987 and one with the main chain of Val-985 (Fig. 3, A and C). This conformation of the juxtamembrane region is further stabilized by hydrogen bonds between the side chain of Asn-1046 (αC) and main chain atoms of Ser-981 (Cys-981 in wild-type IRK) and Val-983 in the juxtamembrane region. Asn-1046 is conserved in insulin and IGF1 receptors and is a lysine in IRR.

FIG. 3. Conformation of the proximal juxtamembrane region in IRK. Stereo views of the proximal juxtamembrane region and the N-terminal kinase lobe from the IRK^{D1132N} structure (A) and the tris-phosphorylated IRK^{Y984F} structure (13) (B) are shown. The view is from above with respect to the view in Fig. 3. The juxtamembrane region is shown in ball-and-stick representation with carbon atoms colored *orange*, nitrogen atoms colored *blue*, and oxygen atoms colored *red*. The side chains of selected residues of the N-terminal kinase lobe are shown in ball-and-stick representation with carbon atoms colored *gray*, nitrogen atoms colored *blue*, and oxygen atoms colored *red*. Semi-transparent van der Waals' surfaces in A indicate hydrophobic packing of Tyr-984 with Leu-1045 and Val-1065. C, schematic diagram (approximate spatial layout) showing the invariant residues in the insulin receptor subfamily that form the Tyr-984 binding pocket. The residue labels are placed alongside the C α atoms of the side chains. The backbone nitrogen atoms of Trp-989 and Ser-1067 are included as well as the carbonyl oxygen of nonconserved Val-985 (*dark gray*). Hydrogen bonds are depicted by *dashed lines*, and van der Waals' interactions (<3.8 Å) with Tyr-984 are depicted as *concentric half-circles*.



In the recent crystal structures of the IGF1 receptor kinase domain in its unphosphorylated (24) or bis-phosphorylated state (25), the tyrosine equivalent to Tyr-984, Tyr-957, is situated in the same hydrophobic pocket as observed for Tyr-984 in the IRK^{D1132N} structure. Of note, Tyr-957 is hydrogen-bonded to conserved Lys-1025 (Lys-1052 in IRK) in the IGF1 receptor kinase structures, whereas in the IRK^{D1132N} structure, Tyr-984 is hydrogen-bonded to conserved Glu-990. This subtle difference in the positioning of Tyr-984/957 in the insulin/IGF1 receptor kinase structures could be a manifestation of the five-residue insertion in the insulin receptor *versus* the IGF1 receptor just prior to Tyr-984 (Fig. 1).

In the unphosphorylated IRK^{Y984F} structure (12), the proximal juxtamembrane region is disposed along α C in approximately the same manner as in the IRK^{D1132N} structure, but the side chain of Phe-984 is exposed to solvent and disordered, and the hydrophobic pocket between α C and the β sheet is instead filled with Val-985. In this juxtamembrane configuration, conserved Trp-989 and Lys-1052 are poorly ordered, and hydrogen bonding between Lys-1052 and conserved Asp-987 is not observed.

The conformation of the proximal juxtamembrane region in the tris-phosphorylated, activated IRK structure (13) is markedly different from the conformations in the unphosphorylated

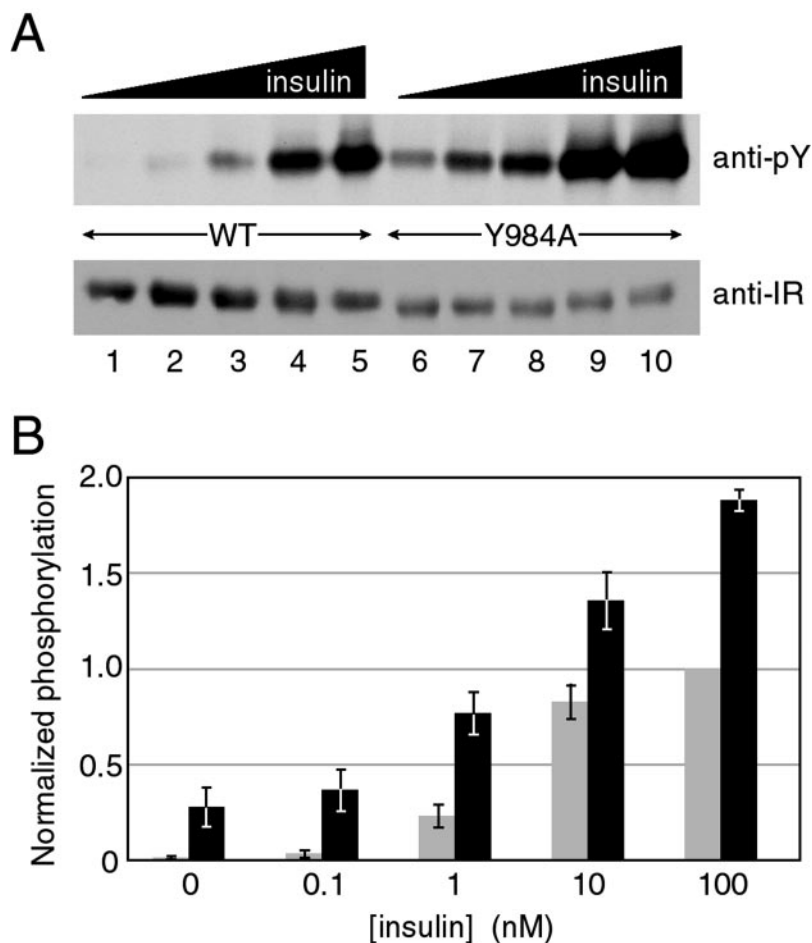
TABLE II
Steady-state kinetics values

Enzyme	$K_{m,ATP}$ <i>mM</i>	$K_{m,peptide}$ <i>mg/ml</i>	k_{cat} <i>min⁻¹</i>
IRK ^{WT} -0P	0.80 ± 0.12	3.96 ± 0.32	2.25 ± 0.10
IRK ^{Y984F} -0P	1.29 ± 0.11	3.51 ± 0.46	9.19 ± 0.62
IRK ^{WT} -3P	0.13 ± 0.01	0.62 ± 0.2	35.4 ± 0.7
IRK ^{Y984F} -3P	0.14 ± 0.01	0.66 ± 0.2	38.2 ± 1.6

Enzyme abbreviations are: IRK^{WT}-0P, unphosphorylated wild-type IRK; IRK^{Y984F}-0P, unphosphorylated Tyr-984 → Phe IRK; IRK^{WT}-3P, tris-phosphorylated wild-type IRK; and IRK^{Y984F}-3P, tris-phosphorylated Tyr-984 → Phe IRK.

FIG. 4. Transient transfection of wild-type and Tyr-984 → Ala mutant insulin receptors in HEK 293T cells.

A, HEK 293T cells were transiently transfected with either wild-type insulin receptors (WT) or insulin receptors bearing the Tyr-984 → Ala mutation (Y984A). Serum-starved cells were stimulated with insulin for 10 min, and the lysates were subjected to SDS-PAGE (7.5%) and Western blotting with an anti-phosphotyrosine antibody (*top blot*) or, from a separate gel, an anti-insulin receptor antibody (*bottom blot*). Insulin concentrations were 0 nM (*lanes 1 and 6*), 0.1 nM (*lanes 2 and 7*), 1.0 nM (*lanes 3 and 8*), 10 nM (*lanes 4 and 9*), or 100 nM (*lanes 5 and 10*). A representative blot is shown. The insulin-stimulated phosphorylation level of endogenous insulin receptors in HEK 293T cells was negligible (data not shown). **B**, quantification of the phosphorylation levels of the wild-type (*gray*) and Tyr-984 → Ala (*black*) insulin receptors as a function of insulin concentration. Anti-phosphotyrosine blots from five independent transient transfection experiments were subjected to densitometry, and the blots were normalized to each other by setting equal to 1.0 the phosphorylation level of the wild-type receptor at the highest insulin concentration (100 nM). Standard deviations are indicated by the *error bars* (except for the wild-type receptor at 100 nM insulin used for normalization). The fold differences in phosphorylation levels (mutant over wild type) at each insulin concentration were: 0 nM, 29.8; 0.1 nM, 11.6; 1.0 nM, 3.3; 10 nM, 1.6; and 100 nM, 1.9. *anti-pY*, anti-phosphotyrosine; *anti-IR*, anti-insulin receptor.



IRK^{D1132N} and IRK^{Y984F} structures. In the activated kinase, the juxtamembrane segment is disengaged from the β sheet- α C cleft (Fig. 3B). This juxtamembrane conformation is similar to that observed in the structure of the tris-phosphorylated form of the IGF1 receptor kinase domain (11), which contained wild-type tyrosine at residue 957 (Tyr-984 equivalent) and crystallized in a different space group. These structural observations indicate that the phosphorylation state of the activation loop dictates the conformation of the proximal juxtamembrane segment.

Steady-state Kinetics Measurements of IRK^{WT} Versus IRK^{Y984F}—To determine whether the observed interactions between the proximal juxtamembrane region, specifically Tyr-984, and residues in the N-terminal kinase lobe affect catalytic activity, the steady-state kinetics parameters (k_{cat} , $K_{m,ATP}$, and $K_{m,peptide}$) were determined for the purified soluble kinase domains, wild-type IRK (IRK^{WT}), and IRK^{Y984F}. Kinetics measurements were performed using a continuous spectrophotometric assay (18, 19) on both the unphosphorylated (basal) and tris-phosphorylated (activated) forms of the enzymes. The data presented in Table II demonstrate that IRK^{WT} is less active

than IRK^{Y984F} in the basal state. The k_{cat} value for IRK^{WT} is ~4-fold lower than for IRK^{Y984F}, with minor differences in the K_m values for ATP and substrate peptide. For tris-phosphorylated IRK^{WT} and IRK^{Y984F}, the k_{cat} and K_m values are essentially equivalent. The increases in k_{cat} upon phosphorylation of IRK^{WT} and IRK^{Y984F} are 15- and 4-fold, respectively, accompanied by a 6-fold decrease in $K_{m,ATP}$.

Transient Transfection of Wild-type and Tyr-984 → Ala Insulin Receptors in Mammalian Cells—Having established from *in vitro* kinetics studies that Tyr-984 represses catalytic activity in the soluble kinase domain, we tested whether full-length insulin receptors bearing the substitution Tyr-984 → Ala are hyperphosphorylated in cells. HEK 293T cells were transiently transfected with either wild-type or Tyr-984 → Ala insulin receptors, and the level of tyrosine phosphorylation of the receptors prior to and following stimulation with insulin was examined. Multiple independent transfection experiments were performed and gave consistent results. The data shown in Fig. 4 demonstrate that tyrosine phosphorylation levels in the Tyr-984 → Ala insulin receptors are considerably elevated over the levels in wild-type receptors, both in the basal state and

upon insulin stimulation. The extent of phosphorylation in the mutant receptors is particularly striking in the absence of insulin, with an average ($n = 5$) fold increase over wild type of ~ 30 . The degree of hyperphosphorylation of mutant *versus* wild-type receptors diminished as the dose of insulin was increased, yet was still ~ 2 -fold at 100 nM insulin (Fig. 4B).

DISCUSSION

At the time of the early structural studies of IRK (12), it was not apparent whether Tyr-984, an invariant tyrosine in the juxtamembrane region of insulin receptor subfamily members, was a site of autophosphorylation, and an expression construct was utilized in which Tyr-984 was replaced by phenylalanine. To elucidate the role of conserved Tyr-984 in insulin receptor function, we expressed and purified an IRK protein from baculovirus-infected insect cells containing tyrosine at residue 984. From initial *in vitro* experiments, it was evident that wild-type IRK underwent autophosphorylation at a slower rate than IRK^{Y984F}. To quantify the catalytic properties of wild-type IRK and IRK^{Y984F}, we measured for each enzyme the steady-state kinetics parameters, K_m (ATP and substrate peptide) and k_{cat} . The results of these experiments (Table II) indicate that k_{cat} is 4-fold lower for wild-type IRK than for IRK^{Y984F} in the basal (unphosphorylated) state.

To determine the mechanism by which wild-type IRK is catalytically repressed in the basal state relative to IRK^{Y984F}, we determined the crystal structure of unphosphorylated IRK containing Tyr-984. In this structure, the juxtamembrane region proximal to the kinase domain (residues 979–988) lies along αC in the N-terminal kinase lobe, with Tyr-984 situated in a hydrophobic pocket between αC and the β sheet in the N-terminal lobe (Fig. 3A).

The interactions of Tyr-984 in the β sheet- αC cleft and a comparison of the αC positions in the unphosphorylated and tris-phosphorylated IRK structures suggest the structural mechanism by which Tyr-984 represses catalytic activity in the basal state. One of the consequences of IRK activation loop autophosphorylation and reconfiguration is the unrestrained rotation of the N-terminal lobe toward the C-terminal lobe (lobe closure) to bind ATP productively (13). In addition to an overall hinge movement of the N-terminal lobe, αC pivots downward toward the C-terminal lobe (Fig. 5A). This independent (from the β sheet) movement of αC facilitates formation of a catalytically important salt bridge between conserved Lys-1020 ($\beta 3$) and conserved Glu-1047 (αC). Importantly, in the activated IRK structure, the proximal juxtamembrane region is disengaged from the β sheet- αC cleft (Figs. 3B and 5). These observations indicate that, in addition to the activation loop, the proximal juxtamembrane segment, anchored by Tyr-984, provides steric restraints preventing αC from assuming its catalytically competent position.

In many protein kinases, αC is a key structural element in the regulation of catalytic activity. For example, in cyclin-dependent kinase 2, αC (or PSTAIRE helix) is not positioned properly to form the conserved lysine-glutamic acid salt bridge (26). Cyclin A binding to cyclin-dependent kinase 2 pushes αC toward the β sheet, resulting in significant stimulation of kinase activity, even in the absence of activation loop phosphorylation (27). In the nonreceptor tyrosine kinase c-Src, intramolecular interactions between the SH3 domain and the SH2-kinase linker stabilize a noncatalytically productive position of αC , contributing to repressed kinase activity (28, 29).

A structural interplay between αC and the activation loop has been documented for c-Src (30). Autophosphorylation of Tyr-416 and concomitant rearrangement of the activation loop disrupts the interactions that stabilize the mispositioning of αC . Conversely, mutations in the $\beta 3$ - αC loop partially activate

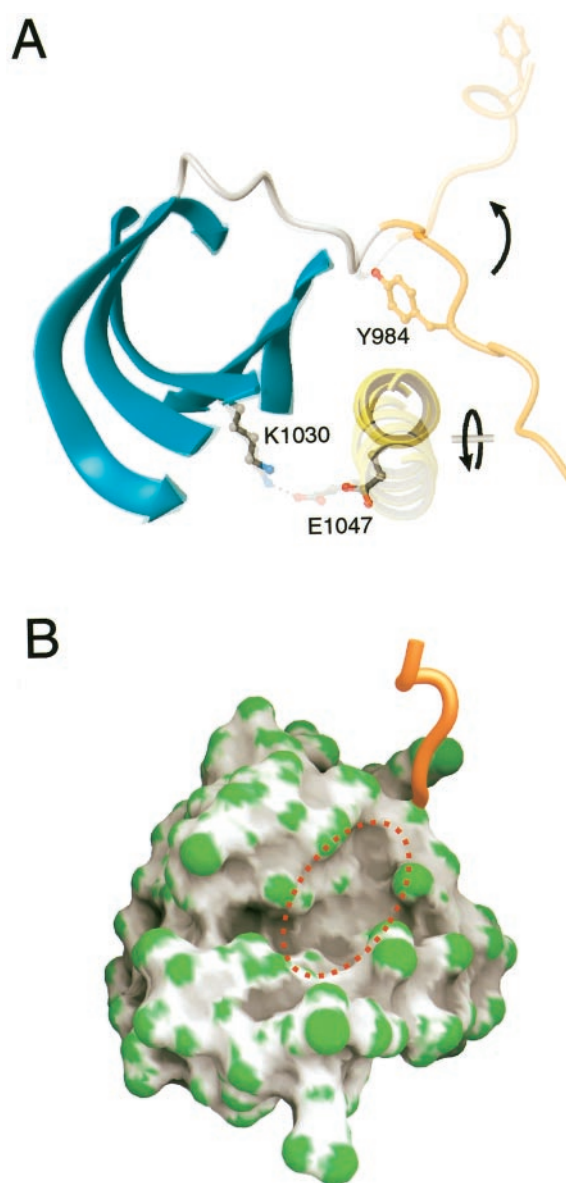


FIG. 5. Positioning of αC and a potential target site for a small molecule activator. A, superposition of the N-terminal lobes of IRK^{D1132N} and tris-phosphorylated IRK (IRK-3P) (13). Only residues in the β sheet were included in the superposition. The N-terminal lobe of IRK-3P is semi-transparent. The kinase-proximal juxtamembrane region is colored orange, with the side chains of Tyr-984 (IRK^{D1132N}) and Phe-984 (IRK-3P) shown explicitly. A hydrogen bond between conserved Lys-1030 and Glu-1047 in IRK-3P is shown by a dashed line. For clarity, the connections between the strands of the β sheet are omitted. The arrows indicate the repositioning of the proximal juxtamembrane segment and αC upon activation loop phosphorylation. B, surface rendering of the N-terminal lobe of IRK-3P colored by curvature: green, high convex curvature; black, high concave curvature. The binding site for a potential small molecule activator of the insulin receptor is shown by a dashed red oval.

c-Src irrespective of Tyr-416 autophosphorylation. Similarly, the structural and kinetic data presented here indicate that partial activation of IRK in the basal state results from disengagement of the proximal juxtamembrane region from the β sheet- αC cleft (*via* mutation of Tyr-984). The observation that, once phosphorylated, wild-type IRK and IRK^{Y984F} have very similar catalytic efficiencies (Table II) implies that the influence of the activation loop on αC positioning is “dominant” over that of the proximal juxtamembrane region.

To determine whether autoinhibition by Tyr-984 as detailed here for the soluble kinase domain is necessary for maintaining

low basal-level phosphorylation in the full-length insulin receptor, we transiently transfected HEK 293T cells with either wild-type insulin receptors or mutant insulin receptors in which Tyr-984 was replaced by alanine. These studies demonstrated that in the absence of insulin, the tyrosine phosphorylation levels of Tyr-984 mutant receptors were significantly elevated (~30-fold) relative to that of wild-type receptors and were ~2-fold elevated at maximal insulin stimulation (Fig. 4). The elevated tyrosine phosphorylation levels in the Tyr-984 → Ala mutant were not due to a decreased susceptibility to dephosphorylation; the wild-type and mutant receptors displayed comparable dephosphorylation kinetics (data not shown).

Interestingly, the activating effect of the Tyr-984 → Ala substitution in the full-length insulin receptor is considerably more robust than for the Asp-1161 → Ala substitution described previously (22). The Asp-1161 → Ala substitution in the activation loop partially relieves activation loop autoinhibition (15), resulting in a sizable increase in catalytic efficiency for the soluble kinase domain in the unphosphorylated state; k_{cat} increases 10-fold, and $K_{m,\text{ATP}}$ decreases 15-fold (22). Yet in the context of the full-length receptor transfected into C2C12 cells (22) or HEK 293T cells (data not shown), a modest effect (~3-fold) on basal-level or insulin-stimulated phosphorylation is observed. In contrast, mutation of Tyr-984 in the soluble kinase domain yields a comparatively small increase in catalytic efficiency (4-fold higher k_{cat}) but results in a substantial increase (~30-fold) in the phosphorylation level of the full-length receptor in unstimulated cells.

The difference in the basal-level phosphorylation states of these two mutant insulin receptors, Tyr-984 → Ala and Asp-1161 → Ala, suggests that, in addition to influencing the position of αC in the kinase domain, the proximal juxtamembrane region plays a key role in the mechanism by which insulin binding to the extracellular α subunits induces a structural rearrangement in the cytoplasmic β subunits. It is conceivable that the interactions between the proximal juxtamembrane segment and αC in the N-terminal kinase lobe are important for maintaining a spatial arrangement of the two kinase domains that limits *trans*-autophosphorylation in the basal state. Loss of these interactions (*via* mutation of Tyr-984) might partially relieve the steric constraints imposed by the extracellular domains (devoid of insulin) on the cytoplasmic domains. The observation that insulin stimulation increases tyrosine phosphorylation of the Tyr-984 → Ala mutant receptor indicates that additional steric restraints in the receptor are still operational.

Importantly, many other RTKs contain either tyrosine at the equivalent position of Tyr-984 in the insulin receptor or another hydrophobic residue at that or a nearby position, which may function similarly to Tyr-984, at least with respect to αC positioning. For example, vascular endothelial growth factor receptor-2 possesses a tyrosine (Tyr-822) at the equivalent position of Tyr-984, which in the crystal structure (31) is disposed similarly to Tyr-984, hydrogen-bonded to Glu-828, the equivalent of Glu-990 in the insulin receptor. In the crystal structure of the kinase domain of fibroblast growth factor receptor-1 (32), Leu-465, one residue N-terminal to the position of Tyr-984 in the insulin receptor, is engaged in the β sheet- αC cleft. Finally, in the crystal structures of Tie2 (33) and EphB2 (34), an isoleucine (Ile-815) or valine (Val-617), respectively, in the proximal juxtamembrane region fulfills this structural role.

Therefore, a similar autoinhibitory mechanism may operate in these and other RTKs, and mutation of the residue positioned in the β sheet- αC cleft would be predicted to result in partial activation. The degree to which the receptor is activated will depend on the relative strength of other autoinhibitory

mechanisms to which that particular RTK is subject (35), *e.g.* activation loop (IRK and MuSK (36)), extended juxtamembrane region (EphB2 (34) and c-Kit (37)), or C-terminal tail (33). Moreover, the constitutive dimeric arrangement of receptors in the insulin receptor subfamily might make receptors in this subfamily particularly sensitive to mutation of conserved Tyr-984, as discussed above.

The structural characterization of the autoinhibitory role of Tyr-984 in the basal state kinase affords a novel strategy for the design of small molecule activators of the insulin receptor. A cell-permeable compound designed to bind in the β sheet- αC cleft and displace Tyr-984 should partially activate the receptor in the absence of insulin and sensitize the receptor in the presence of insulin. The specific target site for such a molecule would be the β sheet- αC cleft as configured in the activated IRK structure (13) (Fig. 5B).

Two compounds capable of stimulating insulin receptor autophosphorylation by acting on the cytoplasmic domain have been reported (38, 39). One of the compounds (L-783,281) modestly elevates insulin receptor autophosphorylation in the absence of insulin, whereas the other compound (TLK16998) potentiates receptor autophosphorylation in the presence of insulin, suggesting two different mechanisms of action (40). Interestingly, L-783,281 and a derivative (41) are of an appropriate size to bind in the β sheet- αC cleft, and L-783,281 was shown to alter the trypsin susceptibility at Lys-1030 (38), not far spatially from Tyr-984 (Fig. 5A). Whether or not the β sheet- αC cleft is the site of action of these compounds, the existence of such small molecule activators, together with the data presented here on the autoinhibitory role of Tyr-984, motivates efforts to design novel insulin receptor activators with potential application to noninsulin-dependent diabetes mellitus.

Acknowledgment—We thank R. Kohanski for reagents, helpful discussions, and manuscript comments.

REFERENCES

- Ullrich, A., Bell, J. R., Chen, E. Y., Herrera, R., Petruzzelli, L. M., Dull, T. J., Gray, A., Coussens, L., Liao, Y. C., Tsubokawa, M., Mason, A., Seeburg, P. H., Grunfeld, C., Rosen, O. M., and Ramachandran, J. (1985) *Nature* **313**, 756–761
- Ebina, Y., Ellis, L., Jarnagin, K., Ederly, M., Graf, L., Clauser, E., Ou, J. H., Masiazk, F., Kan, Y. W., Goldfine, I. D., Roth, R. A., and Rutter, W. J. (1985) *Cell* **40**, 747–758
- Rosen, O. M., Herrera, R., Olowe, Y., Petruzzelli, L. M., and Cobb, M. H. (1983) *Proc. Natl. Acad. Sci. U. S. A.* **80**, 3237–3240
- White, M. F. (1998) *Mol. Cell. Biochem.* **182**, 3–11
- Liu, J., Kimura, A., Baumann, C. A., and Saltiel, A. R. (2002) *Mol. Cell. Biol.* **22**, 3599–3609
- Rajagopalan, M., Neidigh, J. L., and McClain, D. A. (1991) *J. Biol. Chem.* **266**, 23068–23073
- Backer, J. M., Shoelson, S. E., Weiss, M. A., Hua, Q. X., Cheatham, R. B., Haring, E., Cahill, D. C., and White, M. F. (1992) *J. Cell Biol.* **118**, 831–839
- Gustafson, T. A., He, W., Craparo, A., Schaub, C. D., and O'Neill, T. J. (1995) *Mol. Cell. Biol.* **15**, 2500–2508
- Chen, J., Sadowski, H. B., Kohanski, R. A., and Wang, L. H. (1997) *Proc. Natl. Acad. Sci. U. S. A.* **94**, 2295–2300
- Kohanski, R. A. (1993) *Biochemistry* **32**, 5773–5780
- Favelyukis, S., Till, J. H., Hubbard, S. R., and Miller, W. T. (2001) *Nat. Struct. Biol.* **8**, 1058–1063
- Hubbard, S. R., Wei, L., Ellis, L., and Hendrickson, W. A. (1994) *Nature* **372**, 746–754
- Hubbard, S. R. (1997) *EMBO J.* **16**, 5572–5581
- Otwinowski, Z., and Minor, W. (1997) *Methods Enzymol.* **276**, 307–326
- Till, J. H., Ablooglu, A. J., Frankel, M., Bishop, S. M., Kohanski, R. A., and Hubbard, S. R. (2001) *J. Biol. Chem.* **276**, 10049–10055
- Brünger, A. T., Adams, P. D., Clore, G. M., DeLano, W. L., Gros, P., Grosse-Kunstleve, R. W., Jiang, J. S., Kuszewski, J., Nilges, M., Pannu, N. S., Read, R. J., Rice, L. M., Simonson, T., and Warren, G. L. (1998) *Acta Crystallogr. Sect. D Biol. Crystallogr.* **54**, 905–921
- Jones, T. A., Zou, J. Y., Cowan, S. W., and Kjeldgaard, M. (1991) *Acta Crystallogr. Sect. A* **47**, 110–119
- Barker, S. C., Kassel, D. B., Weigl, D., Huang, X., Luther, M. A., and Knight, W. B. (1995) *Biochemistry* **34**, 14843–14851
- Moarefi, I., LaFevre-Bernt, M., Sichi, F., Huse, M., Lee, C. H., Kuriyan, J., and Miller, W. T. (1997) *Nature* **385**, 650–653
- Gruppuso, P. A., Boylan, J. M., Levine, B. A., and Ellis, L. (1992) *Biochem. Biophys. Res. Commun.* **189**, 1457–1463

21. Cann, A. D., and Kohanski, R. A. (1997) *Biochemistry* **36**, 7681–7689
22. Frankel, M., Ablooglu, A. J., Leone, J. W., Rusinova, E., Alexander Ross, J. B., Henrikson, R. L., and Kohanski, R. A. (2001) *Mol. Cell. Biol.* **21**, 4197–4207
23. Ablooglu, A. J., Frankel, M., Rusinova, E., Ross, J. B., and Kohanski, R. A. (2001) *J. Biol. Chem.* **276**, 46933–46940
24. Munshi, S., Kornienko, M., Hall, D. L., Reid, J. C., Waxman, L., Stirdivant, S. M., Darke, P. L., and Kuo, L. C. (2002) *J. Biol. Chem.* **277**, 38797–38802
25. Pautsch, A., Zoephel, A., Ahorn, H., Spevak, W., Hauptmann, R., and Nar, H. (2001) *Structure* **9**, 955–965
26. DeBondt, H. L., Rosenblatt, J., Jancarik, J., Jones, H. D., Morgan, D. O., and Kim, S.-H. (1993) *Nature* **363**, 595–602
27. Jeffrey, P. D., Russo, A. A., Polyak, K., Gibbs, E., Hurwitz, J., Massague, J., and Pavletich, N. P. (1995) *Nature* **376**, 313–320
28. Xu, W., Harrison, S. C., and Eck, M. J. (1997) *Nature* **385**, 595–602
29. Sicheri, F., Moarefi, I., and Kuriyan, J. (1997) *Nature* **385**, 602–609
30. Gonfloni, S., Weijland, A., Kretzschmar, J., and Superti-Furga, G. (2000) *Nat. Struct. Biol.* **7**, 281–286
31. McTigue, M. A., Wickersham, J. A., Pinko, C., Showalter, R. E., Parast, C. V., Tempczyk-Russell, A., Gehring, M. R., Mroczkowski, B., Kan, C. C., Villafranca, J. E., and Appelt, K. (1999) *Struct. Fold. Des.* **7**, 319–330
32. Mohammadi, M., Schlessinger, J., and Hubbard, S. R. (1996) *Cell* **86**, 577–587
33. Shewchuk, L. M., Hassell, A. M., Ellis, B., Holmes, W. D., Davis, R., Horne, E. L., Kadwell, S. H., McKee, D. D., and Moore, J. T. (2000) *Struct. Fold. Des.* **8**, 1105–1113
34. Wybenga-Groot, L. E., Baskin, B., Ong, S. H., Tong, J., Pawson, T., and Sicheri, F. (2001) *Cell* **106**, 745–757
35. Hubbard, S. R. (2002) *Curr. Opin. Struct. Biol.* **12**, 735–741
36. Till, J. H., Becerra, M., Watty, W., Lu, Y., Ma, Y., Neubert, T. A., Burden, S. J., and Hubbard, S. R. (2002) *Structure* **10**, 1187–1196
37. Hirota, S., Isozaki, K., Moriyama, Y., Hashimoto, K., Nishida, T., Ishiguro, S., Kawano, K., Hanada, M., Kurata, A., Takeda, M., Muhammad Tunio, G., Matsuzawa, Y., Kanakura, Y., Shinomura, Y., and Kitamura, Y. (1998) *Science* **279**, 577–580
38. Zhang, B., Salituro, G., Szalkowski, D., Li, Z., Zhang, Y., Royo, I., Vilella, D., Diez, M. T., Pelaez, F., Ruby, C., Kendall, R. L., Mao, X., Griffin, P., Calaycay, J., Zierath, J. R., Heck, J. V., Smith, R. G., and Moller, D. E. (1999) *Science* **284**, 974–977
39. Manchem, V. P., Goldfine, I. D., Kohanski, R. A., Cristobal, C. P., Lum, R. T., Schow, S. R., Shi, S., Spevak, W. R., Laborde, E., Toavs, D. K., Villar, H. O., Wick, M. M., and Kozlowski, M. R. (2001) *Diabetes* **50**, 824–830
40. Li, M., Youngren, J. F., Manchem, V. P., Kozlowski, M., Zhang, B. B., Maddux, B. A., and Goldfine, I. D. (2001) *Diabetes* **50**, 2323–2328
41. Qureshi, S. A., Ding, V., Li, Z., Szalkowski, D., Biazzo-Ashnault, D. E., Xie, D., Saperstein, R., Brady, E., Huskey, S., Shen, X., Liu, K., Xu, L., Salituro, G. M., Heck, J. V., Moller, D. E., Jones, A. B., and Zhang, B. B. (2000) *J. Biol. Chem.* **275**, 36590–36595